

A Level Set Based Eulerian Method for Paraxial Multivalued Traveltimes

Jianliang Qian* Shingyu Leung†

June 24, 2003

Abstract

We apply the level-set methodology to compute multivalued solutions of the paraxial eikonal equation in both isotropic and anisotropic metrics. This paraxial equation is obtained from 2-D stationary eikonal equations by using one of the spatial directions as the artificial evolution direction. The advection velocity field used to move level sets is obtained by the method of characteristics; therefore the motion of level sets is defined in a phase space, and the zero level set yields the location of bicharacteristic strips in the reduced phase space. The multivalued traveltime is obtained from solving another advection equation with a source term. The complexity of the algorithm is $O(N^3 \text{Log} N)$ in the worst case and $O(N^3)$ in the average case, rather than $O(N^4)$ as the typical Lagrangian ray-tracing, where N is the number of the sampling points along one of the spatial directions. Numerical experiments including the well-known Marmousi synthetic model illustrate the accuracy and the efficiency of the Eulerian method.

1 Introduction

The eikonal equation as a first-order nonlinear PDE usually admits more than one weak solution. The concept of viscosity solution developed by Crandall, Evans and Lions [8] and others makes use of the maximum principle for the nonlinear PDE and picks out a unique and stable solution among many weak solutions; physically, this solution corresponds to the first arrival or the least traveltime if the solution of the eikonal equation has the dimension of the time [19]. However, in practice, later arrivals may carry information which is more relevant to applications. In geophysical oil explorations, for example, the first-arrival wavefront may not carry the most energetic part of the wave-field, and later-arrival wavefronts may be more useful for modern high resolution seismic imaging via integral transform in the presence

*Department of Mathematics, UCLA, Los Angeles, CA 90095-1555. Email: qian@math.ucla.edu

†Department of Mathematics, UCLA, Los Angeles, CA 90095-1555. Email: syleung@math.ucla.edu

of strong refraction [12, 20, 22]. In the quantum mechanics, the WKBJ method for the semi-classical limit of the Schrodinger equation needs multivalued phases to construct the asymptotic expansion of the wave field, where the phases are multivalued solutions of an eikonal equation [13, 17, 35].

Naturally one may use the method of characteristics, a Lagrangian formulation, to compute the multivalued solutions of the eikonal equation. However, it suffers from some typical shortcomings of Lagrangian methods, for instance, nonuniform distribution of the solutions in the physical space. The resolution of this is via dynamic addition and removal of rays (characteristics) as computation proceeds at the cost of complicated data structure and bookkeeping [42]. Therefore, one looks for Eulerian formulations for computing multivalued solutions of the eikonal equation. In this regard, a new field, so-called Eulerian geometrical optics, emerged [2] as many researchers have devoted a lot of efforts to developing efficient Eulerian methods for computing multivalued solutions since early 90s. As a result, there are many different approaches in the literature: explicit caustic construction method [1, 3], slowness matching method [39, 40], segment projection method [10], dynamic surface extension method [34, 36], kinetic method for multi-branch entropy solutions [4, 13], co-dimension 2 level-set evolution method [23, 29, 18], Liouville equations for escape parameters [11], to name just a few.

In this paper we propose another level-set based Eulerian method for computing multivalued solutions of the paraxial eikonal equation in both isotropic and anisotropic metrics. The level-set framework provides a natural link from a Lagrangian formulation to an Eulerian formulation. We first derive the ray tracing equation using one of the spatial direction as the running parameter, which corresponds to the paraxial eikonal equation. The ray tracing equation is embedded into a level-set motion equation to define a passive motion for level sets. The multivalued traveltimes is obtained from solving another advection equation with a non-homogeneous source term. The complexity of the algorithm is $O(N^3 \text{Log} N)$ in the worst case and $O(N^3)$ in the average case, rather than $O(N^4)$ as in the typical Lagrangian ray-tracing, where N is the number of the sampling points along one of the spatial directions. This level-set method is different from the ones in [23, 29, 18, 5] in two aspects: on the one hand for a 2-dimensional eikonal equation we use a level-set motion equation defined in the 2-dimensional space rather than the 3-dimensional space; on the other hand, our method yields both locations and multivalued times rather than only the multivalued wavefronts. Of course, the drawback is that the method does not allow overturning, but it is sufficient for many geophysical applications [14, 31] and for some applications in quantum mechanics [28]. Numerical experiments including the well-known Marmousi synthetic model illustrate the accuracy and efficiency of the Eulerian method. In one appendix, we show that our level set formulation is equivalent to the one proposed in the recent work [18].

2 Paraxial Formulation for Isotropic Eikonal equation

Consider the eikonal equation with a point source condition in an isotropic medium which occupies an open, bounded domain $\Omega \subset \mathbf{R}^2$. By isotropy here we mean the wave velocity

has no directional dependence. The equation is as follows,

$$|\nabla_{\mathbf{x}}\tau(\mathbf{x}, \mathbf{x}_s)| = \frac{1}{c(\mathbf{x})}. \quad (1)$$

$$\lim_{\mathbf{x} \rightarrow \mathbf{x}_s} \frac{\tau(\mathbf{x}, \mathbf{x}_s)}{\|\mathbf{x} - \mathbf{x}_s\|} = \frac{1}{c(\mathbf{x}_s)}, \quad \tau \geq 0, \quad (2)$$

where \mathbf{x}_s is the given source point, $c \in C^1(\Omega)$ is the positive velocity. Here $\tau(\mathbf{x}, \mathbf{x}_s)$ denotes the time (“travelttime”) taken by a particle moving at velocity $c(\mathbf{x})$ to travel from the source point \mathbf{x}_s to a target point $\mathbf{x} \in \Omega$. For $\mathbf{x} \neq \mathbf{x}_s$ near \mathbf{x}_s , τ is a differentiable function of both arguments and satisfies the *eikonal equation* (1). However, when \mathbf{x} is sufficiently distant from \mathbf{x}_s and the velocity $c(\mathbf{x})$ is inhomogeneous with spatial position \mathbf{x} , τ is generally a multivalued function of both variables, and cusps and caustics occur with high probabilities [43].

As mentioned above, the concept of viscosity solution can be used to extract a globally single valued solution for the eikonal equation [8]; this solution assigns to each point \mathbf{x} the least of the (possibly many) traveltimes from \mathbf{x}_s to \mathbf{x} . Relying on this concept we may use finite difference schemes to compute the least travelttime stably and efficiently [9, 25, 26, 33, 31, 32]. Although the viscosity concept and related numerical methods provide a natural Eulerian framework for geometrical optics, the drawback is that it provides only first-arrivals while some applications may require all arrival times.

To motivate our derivation from a multivalued Lagrangian framework to a multivalued Eulerian framework, we first derive a single-valued Lagrangian framework from the above viscosity-solution-based single-valued Eulerian framework. Because the rays of geometric optics are the orthogonal trajectories of the wavefronts (level sets of τ) [7], consider the one-parameter family of 2-dimensional wavefronts $\gamma(t)$, where $t \in [\epsilon_0, \infty)$ is time, ϵ_0 is a small number and $\gamma(\epsilon_0)$ is a simple, closed and smooth wavefront. Then near $t = \epsilon_0$, $\gamma(t)$ can be generated by moving $\gamma(\epsilon_0)$ along the normal vector field with speed c depending on position \mathbf{x} . Let $\mathbf{X}(r, t) = (x(r, t), z(r, t))$ be the position vector which parameterizes $\gamma(t)$ by $r: 0 \leq r \leq R$, $\mathbf{X}(0, t) = \mathbf{X}(R, t)$. Then the equations of motion can be written as

$$x_t = c(x, z) \frac{z_r}{\sqrt{x_r^2 + z_r^2}}, \quad z_t = -c(x, z) \frac{x_r}{\sqrt{x_r^2 + z_r^2}}. \quad (3)$$

Given the mapping from $[0, R] \times [\epsilon_0, \infty)$ to \mathbf{R}^2 generated by the moving curve, there exists near $t = \epsilon_0$ an inverse mapping function τ defined by $t = \tau(x, y)$. Then the function τ satisfies the eikonal equation (1), as long as the wavefront stays smooth and non-intersecting [25]. If the wavefront intersects, then the particle tracking system (3) without regridding is linearly ill-posed [25]. However, the monotone numerical method for the viscosity solution of the eikonal equation (1) was well developed which yields a physically relevant solution even if the wavefront self-intersects. In fact, the success of the level set method in the

early stage was more or less attributed to the concept of viscosity solution and related high-order numerical methods [26, 16], so that the topology change and merging can be taken care of automatically when they do occur. On the other hand, it also implies that in the current framework, i.e. Lagrangian formulation (3) and Eulerian formulation (1), it is hard to capture self-intersecting wavefronts unless special care is taken to keep track of some extra parameters, such as amplitude [1] or slowness [39, 40], etc. These extra parameters are essentially used to parameterize the self-intersection, i.e., multivaluedness, and this viewpoint naturally leads to consider phase-space formulations for computing multivalued solutions.

By the method of characteristics for the eikonal equation (1) with the point source condition (2), we have a ray tracing system,

$$\frac{dx}{dt} = c \sin \theta \quad (4)$$

$$\frac{dz}{dt} = c \cos \theta \quad (5)$$

$$\frac{d\theta}{dt} = \sin \theta \frac{\partial c}{\partial z} - \cos \theta \frac{\partial c}{\partial x} \quad (6)$$

with initial conditions

$$x|_{t=0} = x_s \quad (7)$$

$$z|_{t=0} = z_s \quad (8)$$

$$\theta|_{t=0} = \theta_s \quad (9)$$

where $\mathbf{x} = (x, z)$, $\mathbf{x}_s = (x_s, z_s)$ and θ_s varies from $-\pi$ to π . This is a multivalued Lagrangian formulation because even though the rays in the phase space (x, z, θ) may never intersect, the projected rays in the physical space (x, z) may intersect.

In some applications, for example, wave propagation in reflection seismics [6], the traveltimes of interest are carried by the so-called sub-horizontal rays [14, 38, 31], where sub-horizontal means ‘‘oriented in the positive z -direction’’; see also [28] for an example in quantum mechanics. A convenient characterization for sub-horizontal rays is that

$$\frac{dz}{dt} \geq c \cos \theta_{\max} > 0. \quad (10)$$

This inequality holds for rays making an angle θ with the vertical satisfying $|\theta| \leq \theta_{\max} < \frac{\pi}{2}$.

To be specific, consider

$$\Omega = \{(x, z) : x_{\min} \leq x \leq x_{\max}, 0 \leq z \leq z_{\max}\} \quad (11)$$

and assume that the source is located on the surface: $x_{\min} \leq x_s \leq x_{\max}$ and $z_s = 0$. By the sub-horizontal condition we can use depth as the running parameter so that we have a reduced system

$$\frac{dx}{dz} = \tan \theta \quad (12)$$

$$\frac{d\theta}{dz} = \frac{1}{c} \left(\frac{\partial c}{\partial z} \tan \theta - \frac{\partial c}{\partial x} \right) \quad (13)$$

with

$$x|_{z=0} = x_s \quad (14)$$

$$\theta|_{z=0} = \theta_s \quad (15)$$

where now θ_s varies from $-\theta_{\max} \leq \theta \leq \theta_{\max} < \frac{\pi}{2}$. In addition, the traveltime is computed by integrating

$$\frac{dt}{dz} = \frac{1}{c \cos \theta} \quad (16)$$

with

$$t|_{z=0} = 0. \quad (17)$$

This ray tracing system (12-15) is a multivalued Lagrangian formulation defined in the reduced phase space $(z; x, \theta)$. Actually, the ray tracing system can be obtained by applying the method of characteristics to the paraxial eikonal equation

$$\frac{\partial \tau}{\partial z} = H \left(x, z, \frac{\partial \tau}{\partial x} \right) = \sqrt{\max \left(\frac{1}{c^2} - \left(\frac{\partial \tau}{\partial x} \right)^2, \frac{\cos^2 \theta_{\max}}{c^2} \right)}, \quad (18)$$

which in turn comes from enforcing the sub-horizontal condition in the eikonal equation (1); see [40] for a theoretical justification.

As we will see, since the ray tracing system (12), (13) is formulated in a reduced phase space, we may use a 2-dimensional level set motion equation to move the initial curve deduced from the initial condition and the curves moved will not self-intersect because they are defined in the reduced phase space.

3 Paraxial formulation for anisotropic eikonal equation

For general anisotropic media in which wave propagation velocities have both spatial and directional dependence, we may also formulate paraxial eikonal equations by enforcing a version of sub-horizontal condition.

To illustrate the idea behind our approach, we consider the two-dimensional anisotropic eikonal equation only; please see [29] for a detailed derivation of 3-D anisotropic eikonal equations. Consequently, we denote the 2-D anisotropic eikonal equation as

$$F(x, z, p_1, p_3) = 0, \quad (19)$$

where F is a function depending on the anisotropic medium under consideration. Parameterize the slowness vector by

$$p_1 = \frac{\sin \theta}{V(x, z, \theta)}, \quad p_3 = \frac{\cos \theta}{V(x, z, \theta)}, \quad (20)$$

where θ is known as the phase angle, varying from $-\pi$ to π , and V as the phase velocity solving an eigenvalue problem [29] and selecting different wave modes. Applying the method of characteristics to equation (19) yields

$$\frac{dx}{dt} = \left(p_1 \frac{\partial F}{\partial p_1} + p_3 \frac{\partial F}{\partial p_3} \right)^{-1} \frac{\partial F}{\partial p_1}, \quad (21)$$

$$\frac{dz}{dt} = \left(p_1 \frac{\partial F}{\partial p_1} + p_3 \frac{\partial F}{\partial p_3} \right)^{-1} \frac{\partial F}{\partial p_3}, \quad (22)$$

$$\frac{dp_1}{dt} = - \left(p_1 \frac{\partial F}{\partial p_1} + p_3 \frac{\partial F}{\partial p_3} \right)^{-1} \frac{\partial F}{\partial x}, \quad (23)$$

$$\frac{dp_3}{dt} = - \left(p_1 \frac{\partial F}{\partial p_1} + p_3 \frac{\partial F}{\partial p_3} \right)^{-1} \frac{\partial F}{\partial z}, \quad (24)$$

where the evolution parameter t has the dimension of time. To obtain an equation for $\frac{d\theta}{dt}$, we differentiate the equations in (20), arriving at

$$\frac{dp_1}{dt} = \frac{V \cos \theta - \frac{\partial V}{\partial \theta} \sin \theta}{V^2} \frac{d\theta}{dt} - \frac{\sin \theta}{V^2} \left(\frac{\partial V}{\partial x} \frac{dx}{dt} + \frac{\partial V}{\partial z} \frac{dz}{dt} \right), \quad (25)$$

$$\frac{dp_3}{dt} = \frac{-V \sin \theta - \frac{\partial V}{\partial \theta} \cos \theta}{V^2} \frac{d\theta}{dt} - \frac{\cos \theta}{V^2} \left(\frac{\partial V}{\partial x} \frac{dx}{dt} + \frac{\partial V}{\partial z} \frac{dz}{dt} \right). \quad (26)$$

Thus, solving the above equations for $\frac{d\theta}{dt}$ and substituting in (23) and (24) gives us

$$\frac{d\theta}{dt} = \left(p_1 \frac{\partial F}{\partial p_1} + p_3 \frac{\partial F}{\partial p_3} \right)^{-1} \left(V \frac{\partial F}{\partial x} \cos \theta - V \frac{\partial F}{\partial z} \sin \theta \right). \quad (27)$$

Equations (21), (22) and (27) give us the ray tracing system which may be solved with suitable initial conditions as (7), (8) and (9).

The condition for sub-horizontal rays is

$$\frac{dz}{dt} = \left(p_1 \frac{\partial F}{\partial p_1} + p_3 \frac{\partial F}{\partial p_3} \right)^{-1} \frac{\partial F}{\partial p_3} > 0, \quad (28)$$

which may be enforced easily in the reduced phase space for different wave modes. This implies that we may use the depth variable as the running parameter along the ray so that we have

$$\frac{dx}{dz} = \frac{\partial F}{\partial p_1} \left(\frac{\partial F}{\partial p_3} \right)^{-1} \quad (29)$$

$$\frac{d\theta}{dz} = \left(\frac{\partial F}{\partial p_3} \right)^{-1} \left(V \frac{\partial F}{\partial x} \cos \theta - V \frac{\partial F}{\partial z} \sin \theta \right), \quad (30)$$

augmented with initial conditions (14) and (15).

Similar to the isotropic case, the traveltime is computed by integrating

$$\frac{dT}{dz} = p_3 + p_1 \frac{dx}{dz}, \quad (31)$$

with the initial condition (17).

4 Level Set Formulation

As we mentioned above, we treat z as an artificial time variable. Now, if we define $\phi = \phi(z, x, \theta)$ such that the zero level set, $\{(x(z), \theta(z)) : \phi(z, x(z), \theta(z)) = 0\}$, gives the location of the reduced bicharacteristic strip $(x(z), \theta(z))$ at z , then we may differentiate the zero level set equation with respect to z to obtain

$$\phi_z + u\phi_x + v\phi_\theta = 0, \quad (32)$$

with

$$u = \frac{dx}{dz} \quad \text{and} \quad v = \frac{d\theta}{dz}, \quad (33)$$

which are given by the ray equations (12-13) or (29-30). In essence, we embed the ray tracing equations as the velocity field, $\mathbf{u} = (u, v)$, into the level set equation which governs the motion of the bicharacteristic strips in the phase space.

The initial condition for the level set motion equation (32) is taken to be

$$\phi|_{z=0} = \phi(0, x, \theta) = x - x_s, \quad (34)$$

which is obtained from initial conditions (14) and (15). This is a signed distance function, satisfying $|\nabla_{x,\theta}\phi| = 1$, to the initial phase space curve

$$\{(x, \theta) : x = x_s, -\theta_{\max} \leq \theta \leq \theta_{\max}\} \quad (35)$$

in the reduced phase space

$$\Omega_p = \{(x, \theta) : x_{\min} \leq x \leq x_{\max}, -\theta_{\max} \leq \theta \leq \theta_{\max}\}. \quad (36)$$

The initial curve partitions Ω_p into two sub-domains represented by $\{(x, \theta) : \phi(0, \cdot, \cdot) < 0\}$ and $\{(x, \theta) : \phi(0, \cdot, \cdot) > 0\}$. Afterwards, the level set motion equation takes over and moves this initial curve as z varies, and the zero level set of ϕ at z gives the location of the new curve which still partitions Ω_p into two sub-domains. Since the initial curve defines an implicit function between x and θ , where θ is a multivalued function of x , the new curve shares the same property. Therefore, for fixed z , for some x^* 's we may have more than one θ^* such that $\phi(z, x^*, \theta^*) = 0$. This essentially tells us where the solutions are multivalued.

To determine the arrival-time of the ray from the above level set equation, we now derive a corresponding equation governing the evolution of traveltime. By the sub-horizontal

condition in the paraxial formulation and the ray equation (16) or (31), let $F_{\mathbf{u}}(x, \theta; z)$ be the flow generated by the velocity field \mathbf{u} in the phase space (x, θ) along the z -direction. Then we can write

$$\frac{dT}{dz}(z, F_{\mathbf{u}}(x, \theta; z)) = \frac{1}{c \cos \theta} \quad (37)$$

in the isotropic case and

$$\frac{dT}{dz}(z, F_{\mathbf{u}}(x, \theta; z)) = p_3 + p_1 \frac{dx}{dz} \quad (38)$$

in the anisotropic case. Therefore, having $t = T(z, x, \theta)$, we get the following advection equation

$$\frac{dt}{dz} = \frac{dT}{dz} = T_z + uT_x + vT_\theta = \frac{1}{c \cos \theta} \quad (39)$$

for isotropic traveltimes and

$$\frac{dt}{dz} = \frac{dT}{dz} = T_z + uT_x + vT_\theta = p_3 + p_1 \frac{dx}{dz} \quad (40)$$

for anisotropic traveltimes.

The initial condition for T is specified according to the initial condition (17):

$$T|_{z=0} = T(0, x, \theta) = 0, \quad (41)$$

which is consistent with the initial condition (34).

5 Implementation

We will give full details on implementing the level set Eulerian method for isotropic eikonal equations only.

5.1 Boundary conditions and an algorithm

Non-reflective boundary conditions are used for the level set equation. This can make sure the information outside the domain Ω_p will not interfere with the zero level set inside the computational domain. The boundary conditions for the traveltime equation are determined using the local information from the characteristics system. We first invert equation (4) and (6) locally and get

$$\frac{\partial T}{\partial x} = \frac{1}{c \sin \theta}, \quad (42)$$

which is used for boundaries $x = x_{\min}$ and $x = x_{\max}$, and

$$\frac{\partial T}{\partial \theta} = \left(\sin \theta \frac{\partial c}{\partial z} - \cos \theta \frac{\partial c}{\partial x} \right)^{-1}, \quad (43)$$

which is used for boundaries $\theta = -\theta_{\max}$ and $\theta = \theta_{\max}$. Then the values of T on the boundaries will be obtained by solving the above equations by treating them as ODE's using method like Adams' Extrapolation formula.

With above ingredients in place, we summarize the first algorithm for determining the multivalued traveltimes for all x at some depth z^* .

Algorithm 1:

- I. Solve the level set equation (32) and the traveltime equation (39) up to z^* with the velocity field generated by the ray equations (12), (13).
- II. For all x ,
 - i. determine **all** θ_i such that $\phi(z^*, x, \theta_i) = 0$ ($i = 1, \dots$) by root finding;
 - ii. determine $T(z^*, x, \theta_i)$ ($i = 1, \dots$) by interpolation.

In Step I, the level set equation and the traveltime equation are decoupled and can be solved separately. The spacial derivatives are approximated by fifth order WENO-Godunov scheme [16] while third order TVD-RK method [26] can be used for the time derivatives. Both level set equation (32) and traveltime equation (39) are linear, hence the CFL step Δz can be chosen by

$$\Delta z \leq C \frac{\min(\Delta x, \Delta \theta)}{\max(\sqrt{u^2 + v^2})}, \quad (44)$$

where Δx and $\Delta \theta$ are mesh sizes along x and θ directions respectively, and C is a CFL number taken to be 0.6. For the root-finding and the interpolation in Step II, we can simply use any non-oscillatory interpolation scheme, for example, linear interpolation or ENO reconstruction.

5.2 Regularizations

Initially at $z = 0$, we have a signed distance function satisfying $|\nabla \phi| = 1$, so that the level sets, i.e., contours, of ϕ are equally spaced. However, as z varies the level set equation is solved and the level set function is updated; in general the level set function is no longer equally spaced because of the underlying inhomogeneous velocity field, even though the zero level set of ϕ at z , the curve that we are interested in, is moving at the correct velocity. This implies that ϕ may develop steep and flat gradients at or near the zero level set, making the computed curve locations and further computations inaccurate, which does happen in Algorithm 1.

In fact, numerically, if Algorithm 1 is implemented straightforwardly, then the obtained multivalued solution is inaccurate. Therefore, we propose the following regularization procedure which consists of reinitialization and orthogonalization.

To restore the equally spaced property for the level sets, the usual way is to make ϕ a signed distance function without moving the zero level set of ϕ appreciably. This can be

achieved through the so-called reinitialization by solving the following equation to steady state $\tilde{\phi}_\infty$ [37, 15, 27, 24]:

$$\frac{\partial \tilde{\phi}}{\partial \xi} + \text{sgn}(\phi)(|\nabla \tilde{\phi}| - 1) = 0 \quad (45)$$

$$\tilde{\phi}|_{\xi=0} = \phi(z, \cdot, \cdot) \quad (46)$$

where sgn is a smoothed signum function

$$\text{sgn}(\phi) = \frac{\phi}{\sqrt{\phi^2 + |\nabla \phi|^2 \Delta x \Delta \theta}}. \quad (47)$$

The steady state $\tilde{\phi}_\infty$ has the same zero level set as $\phi(z, \cdot, \cdot)$ within a certain accuracy since $\tilde{\phi}$ does not move on the zero level set of ϕ . Moreover, at the steady state $\tilde{\phi}_\infty$ is a signed distance function since $|\nabla \tilde{\phi}_\infty| = 1$. The reinitialization step is to use $\tilde{\phi}_\infty$ instead of $\phi(z, \cdot, \cdot)$ as the initial condition at z for solving the level set motion equation to the next stage. To achieve the steady state we usually need only evolve equation (45) for a few pseudo steps. How often we should invoke the reinitialization step is a subtle issue; see [27, 24] for some discussions. In our implementation, we invoke the reinitialization at every z step so that we have a better-behaved function for determining the values θ_i in Step II of Algorithm 1.

Even with careful implementation of the above reinitialization procedure, the location of the zero level set may still be shifted by an amount less than one grid cell. This is harmless for the visualization purpose of the location of the ray. However, because the solution from the traveltine equation (39) would typically vary a lot near the corresponding location of the zero level set of ϕ , this shift makes the results from the interpolation in Step II highly inaccurate.

Because we are only interested in the value of T where $\phi = 0$, we propose the following orthogonalization procedure

$$\frac{\partial \tilde{T}}{\partial \xi} + \text{sgn}(\phi) \left(\frac{\nabla \phi}{|\nabla \phi|} \cdot \nabla \tilde{T} \right) = 0, \quad (48)$$

$$\tilde{T}|_{\xi=0} = T(z, \cdot, \cdot) \quad (49)$$

which, theoretically, preserves the values of T where $\phi = 0$ but changes them elsewhere such that the new T would not vary too much near the desired region. At the steady state, $\nabla \phi \cdot \nabla \tilde{T} = 0$. Equation (48) may also be viewed as an extension procedure; namely, we extend the values of T on the zero level set of ϕ along the normals of the zero level set of ϕ ; see [27, 24]. This generally makes T discontinuous since lines normal to the zero level set will eventually intersect somewhere away from the zero level set. Even if the location of the zero level set may be shifted, the effect to the interpolation will still be acceptable.

Similar to the reinitialization in ϕ , we only need to apply the above equation to T once several z -steps. This makes the regularization procedure efficient, simple to implement and robust.

Incorporating the regularization procedure into Algorithm I, we have an improved algorithm.

Algorithm 2:

- I. Initialization: given N_z , N_x and N_θ : $\Delta z = \frac{z_{\max}}{N_z-1}$, $\Delta x = \frac{x_{\max}-x_{\min}}{N_x-1}$ and $\Delta\theta = \frac{2\theta_{\max}}{N_\theta-1}$; initialize ϕ and T at $z = 0$.
- II. For $k = 1$ to N_z :
 1. March one Δz step from $(k-1)\Delta z$ to $k\Delta z$ by solving the level set equation (32) and reinitializing the level set motion by solving (45) at every intermediate z -step.
 2. March one Δz step from $(k-1)\Delta z$ to $k\Delta z$ by solving the traveltime equation (39).
 3. Orthogonalize T and ϕ by solving equation (48).
 4. For $x = (j-1)\Delta x, j = 1, \dots, N_x$,
 - i. determine **all** θ_i such that $\phi(k\Delta z, x, \theta_i) = 0$ ($i = 1, \dots$) by root finding;
 - ii. determine $T(k\Delta z, x, \theta_i)$ ($i = 1, \dots$) by interpolation.

Since the reinitialization step is usually invoked for a fixed number of pseudo-steps (from 1 to 4 pseudo-steps in our numerical examples presented below), the above algorithm in the average case has the complexity $O(N^3)$ where $N_z = N_x = N_\theta = N$ is assumed. In the worst case, if the reinitialization step is invoked for indefinite pseudo-steps, the above algorithm has the complexity $O(N^3 \text{Log} N)$.

6 Numerical Experiments

For the first three examples here, we put a point source at the origin and the velocity functions $c(x, z)$ are both C^∞ . The fourth example, the synthetic Marmousi model, is a more challenging one where the velocity function is given only as a sampled function.

In all the examples the computational domain is chosen to be

$$\Omega_p = \{(x, \theta) : -1 \leq x \leq 1, -\frac{9\pi}{20} \leq \theta \leq \frac{9\pi}{20}\}. \quad (50)$$

Accordingly, the Marmousi velocity will be rescaled to the above computational domain. The last example is an anisotropic model which consists of three different wave modes; one of the wave modes has the so-called instantaneous singularity.

6.1 Constant velocity model

When the velocity c is constant, the analytic solution for the traveltime is known so that we can study the accuracy and the convergence order of the proposed Eulerian method. We compute the traveltime up to $z=1.0\text{km}$ with different options of regularization procedures to

Δx	l_1 error	l_1 order	l_2 error	l_2 order	l_∞ error	l_∞ order
0.2	0.01759847		0.01303857		0.01211053	
0.1	0.00436508	2.0113	0.00323837	2.0094	0.00349637	1.7923
0.05	0.00095763	2.1884	0.00074329	2.1232	0.00079357	2.1394
0.025	0.00025030	1.9358	0.00018810	1.9823	0.00021538	1.8814

Table 1: Accuracy and convergence order without either reinitialization or orthogonalization

Δx	l_1 error	l_1 order	l_2 error	l_2 order	l_∞ error	l_∞ order
0.2	0.03100681		0.02516430		0.02906151	
0.1	0.00696316	2.1547	0.00539520	2.2216	0.00589767	2.3008
0.05	0.00145892	2.2548	0.00122996	2.1330	0.00181473	1.7003
0.025	0.00039597	1.8814	0.00032670	1.9125	0.00054628	1.7320

Table 2: Accuracy and convergence order without orthogonalization but 2 reinitialization pseudo steps at each z -step

see how reinitialization and orthogonalization affect the accuracy and the convergence order of the method.

Table 1 shows the clean second-order accuracy and convergence in l_1 , l_2 and l_∞ norms without either reinitialization or orthogonalization. This is expected because the linear interpolation is used to extract traveltimes gives us second-order accuracy only, even though the level set equation and the traveltime equation are solved to third order accuracy.

Table 2 also shows the second order convergence in different norms without orthogonalization but with two reinitialization pseudo steps at each z -step. This shows that the reinitialization procedure alone does not move the zero level set too much so that the accuracy is not affected appreciably.

Table 3 shows the second order convergence in different norms without reinitialization but with two orthogonalization pseudo steps at each z -step. This shows that the orthogonalization procedure improves the behavior of the traveltime field near the zero level set so that the traveltime accuracy is enhanced greatly.

Table 4 shows the second order convergence is lost if both reinitialization and orthogonalization are invoked; however, compared to the results in Table 1, the accuracy of the computed traveltime is not lost. This indicates that by reinitialization and orthogonalization we are solving a PDE which is a high order perturbation of the original PDE.

6.2 Wave guide

The velocity function is

$$c(x, z) = 1.1 - \exp(-0.5x^2). \quad (51)$$

Δx	l_1 error	l_1 order	l_2 error	l_2 order	l_∞ error	l_∞ order
0.2	0.01439364		0.01408975		0.01733903	
0.1	0.00152187	3.2415	0.00145152	3.2790	0.00254247	2.7697
0.05	0.00031820	2.2578	0.00030611	2.2454	0.00049173	2.3702
0.025	0.00006929	2.1992	0.00006502	2.2350	0.00012570	1.9678

Table 3: Accuracy and convergence order without reinitialization but 2 orthogonalization pseudo steps at each z -step

Δx	l_1 error	l_1 order	l_2 error	l_2 order	l_∞ error	l_∞ order
0.2	0.00669519		0.00617415		0.00883762	
0.1	0.00096458	2.7951	0.00124892	2.3055	0.00264324	1.7413
0.05	0.00021842	2.1427	0.00022786	2.4544	0.00060027	2.1386
0.025	0.00009502	1.2007	0.00014089	0.6936	0.00057516	0.0616

Table 4: Accuracy and convergence order with 2 reinitialization pseudo steps and 2 orthogonalization pseudo steps at each z -step

The function is symmetric with respect to $x = 0$, and we also expect the same type of symmetry in the traveltimes.

Figure 1 shows the traveltimes we obtained using only 40×40 grids in the x - θ space. The solutions here show the traveltimes at z equals 0.8, 1.2, 1.6 and 2.0. The solutions are symmetric as expected. Another thing we can check from the graphs is the traveltimes for the particular ray with $\theta = 0$. This means the ray will always travel in a media with $c(0, z) = 0.1$ exactly on the z^+ -axis from the origin. The traveltimes for that particular ray is given by $T = z/0.1$, and this matches with the computations.

Figure 2 shows the zero level set overlaying the traveltimes field at $z = 0.8, 1.2, 1.6$ and 2.0 respectively. The dashed line is the location of the zero level set and the solid lines are the contour plot of the traveltimes function T . There are discontinuities in the traveltimes field coming from the orthogonalization procedure, where the normals of the zero level set intersect. However, it is reminded that we only use the information near the dashed line and the jump in T will not hurt our interpolation computations. Figure 2 also shows that the contours are perpendicular to the zero level set as designed. As z varies, the zero level set is advected so that it has more turnarounds and the number of traveltimes arrivals increases from 1 to 3.

6.3 Sinusoidal model

This example is adapted from the sinusoidal waveguide model proposed in [39, 40], and the velocity function is given by

$$c(x, z) = 1 + 0.2 \sin(0.5\pi z) \sin[3\pi(x + 0.55)]. \quad (52)$$

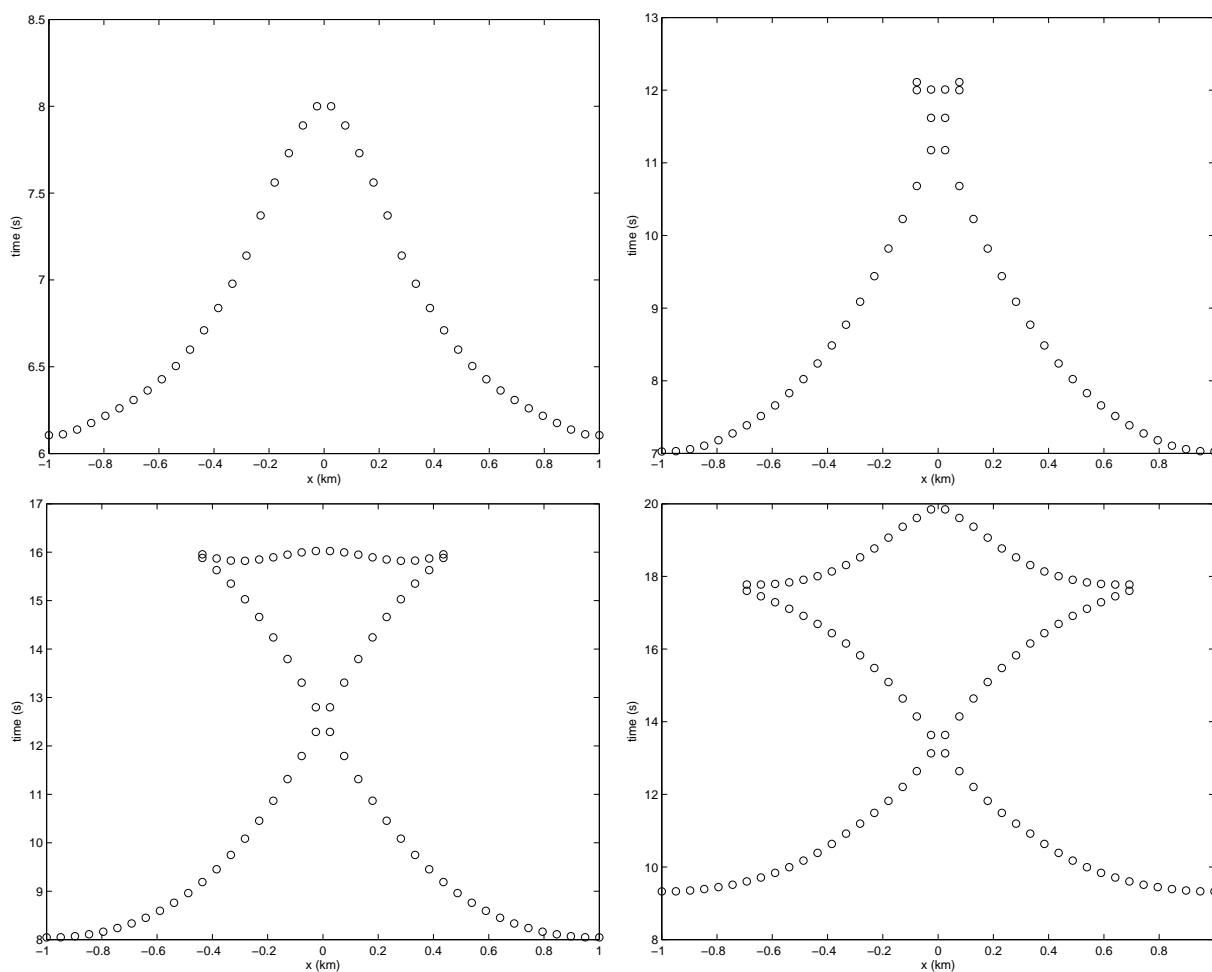


Figure 1: Multivalued traveltimes by the level set method for $z=0.8, 1.2$ (in the upper row), 1.6 and 2.0 in the wave guide model. The multivalued solutions are developed as z increases.

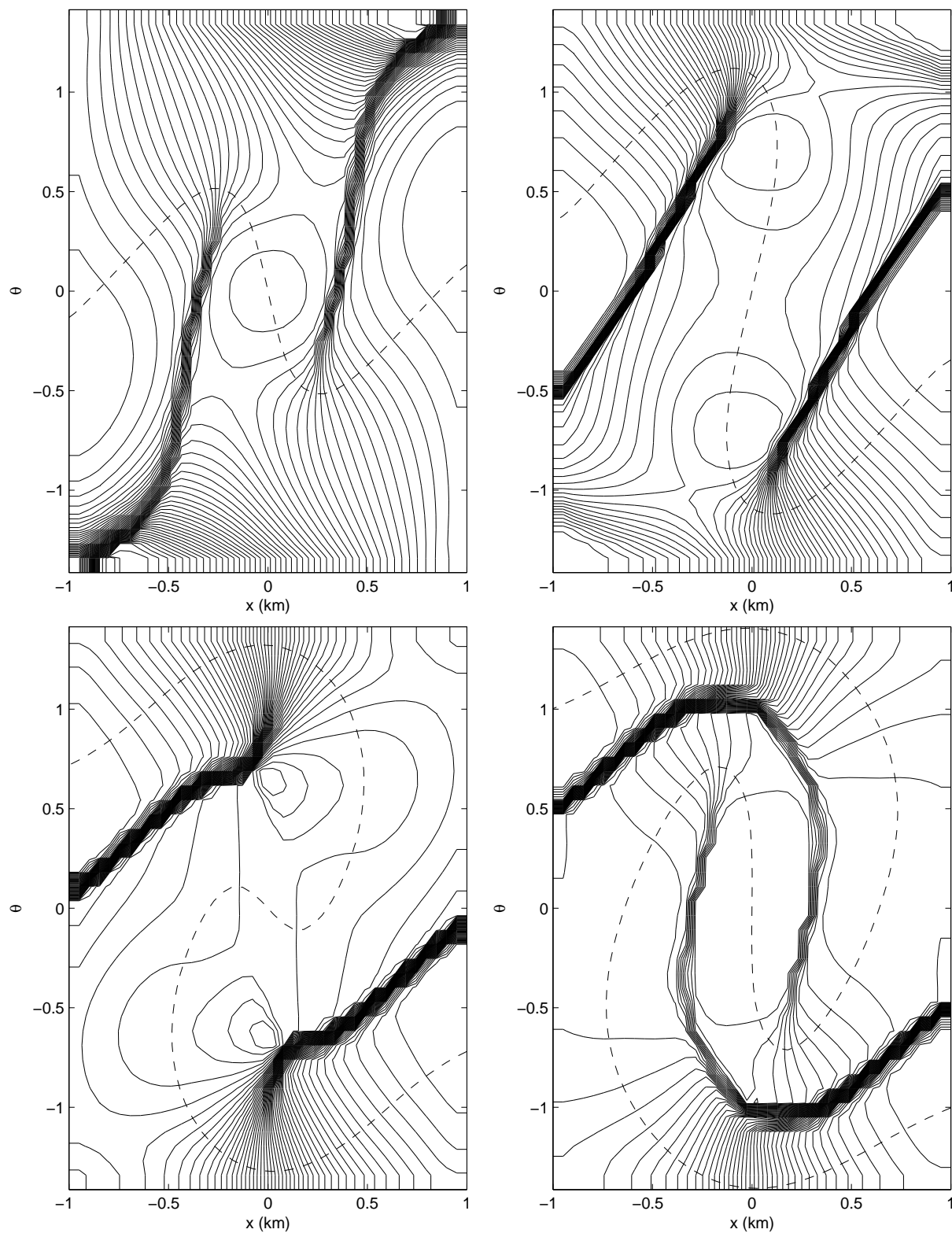


Figure 2: The zero level set overlaid on contours of time field T in the wave guide model.

Computational results using 120 by 120 grid in x - θ space are given in Figures 3 to 5. In these computations the number of pseudo steps in the reinitialization are set to be 1. Figure 3 shows that the triplications in the traveltimes developed at $z = 0.4, 1.0, 1.2$ and 1.8 are clearly captured by the level set Eulerian method. Figure 4 shows the zero level set overlaying the traveltimes field at $z = 1.2$ and 1.8 ; the zero level set is orthogonal to the contours of T . Note that there are five traveltimes at some locations x .

To check the accuracy of the calculated multivalued traveltimes, we compare the results with the solution obtained by solving the ray tracing equations (12), (13) directly at $z = 2.0$; the comparison is shown in Figure 5. The solid line is the solution using our level set formulation while the circles represent the ray-tracing solution. The solutions match with each other; however, the ray tracing Lagrangian method failed to assign traveltimes to some locations, leaving some shadow zones in the domain, but the level set Eulerian method here has no such problem at all, and every location was assigned at least one traveltimes, i.e., the first-arrival traveltimes.

To study the convergence order of the method, we also compute the solution up to $z = 2.0$ km using 240 by 240 grids in x - θ space. The results are shown in Figure 6. Compared to the results in Figure 5, the accuracy is first order. This is not surprising because the reinitialization step essentially implies that we are solving an equation which is high order perturbation of the original equation.

6.4 Synthetic Marmousi model

This example is the Marmousi model from the 1996 INRIA Workshop on Multi-arrival Traveltimes. The calibration data used here were computed by Dr. Klimes and can be found at <http://www.caam.rice.edu/~benamou/traveltimes.html>. This is a synthetic model which will challenge the level-set method used here, and we will study this model carefully.

The original Marmousi model is sampled on a 24m by 24m grid, consisting of 384 samples in x -direction and 122 samples in the z -direction; therefore the model dimension is 9.192km long in x -direction and 2.904km deep in z -direction. In the computational results presented here, we use a portion of Marmousi model, i.e., a window from 4.8km to 7.2km in x -direction and from 0km to 2.904km in z -direction. The source is located at $x=6.0$ km and $z=2.8$ km. The purpose is to compute (possibly multivalued) traveltimes for those sampling points, i.e. the receivers from 200 to 300 on the surface $z=0.0$ km.

In the first run, we used 100 by 200 grid in x - θ space with $\Delta x=24$ m and $\theta_{\max}=\frac{9\pi}{20}$. The computed traveltimes at $z=0.0$ km and the comparison with the ray tracing solution are shown on Figure 7. The ray tracing data used to calibrate the computed Eulerian solutions are presumably accurate. As we can see from Figure 7, the computed Eulerian solution is consistent with the ray tracing solution, being able to capture most of the structure of the multivalued solution, but it failed to resolve some fine details, especially the two traveltimes branches located from receivers 260 to 280, where those two branches are very close to each other. Figure 8 tells us why the level set method failed in that region. Figure 8 shows that the zero level set and its overlaying on the traveltimes field in the reduced phase space. From the ray tracing solution we know that receivers 260 to 280 should have three arrivals, but

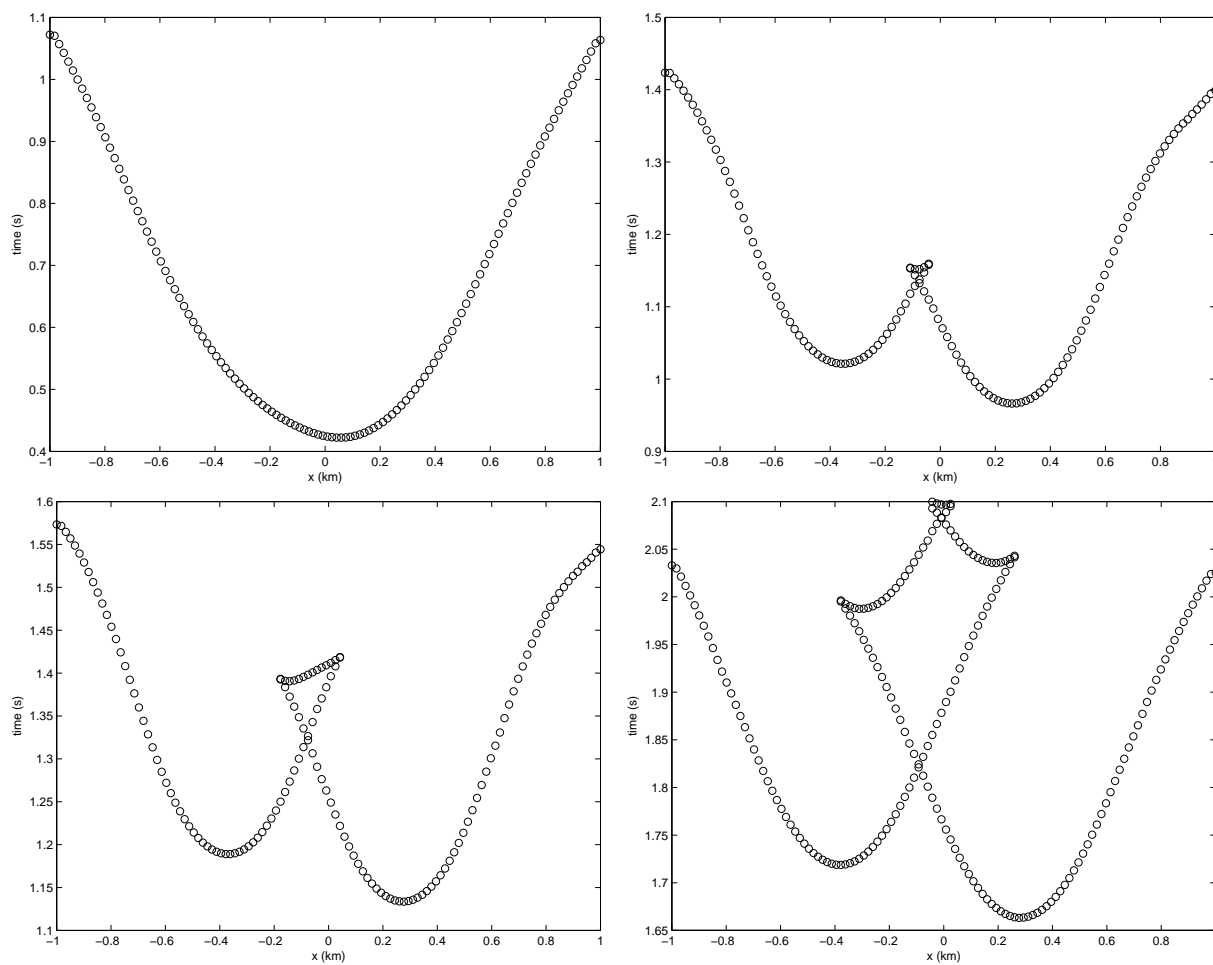


Figure 3: Traveltimes for $z=0.4, 1.0$ (in the upper row), 1.2 and 1.8 in Sinusoidal model. Notice that there are five traveltimes for some points near $x=0$.

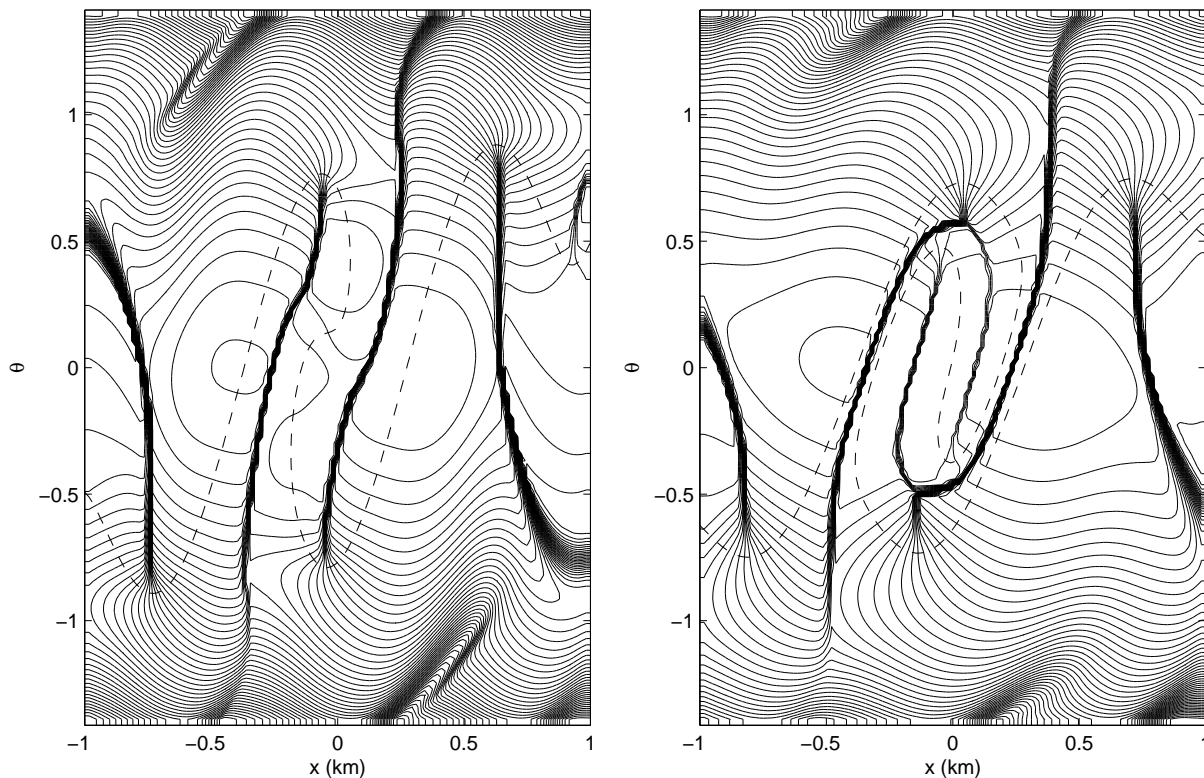


Figure 4: The zero level set and the contour of T at $z = 1.2$ and 1.8 in Sinusoidal model.

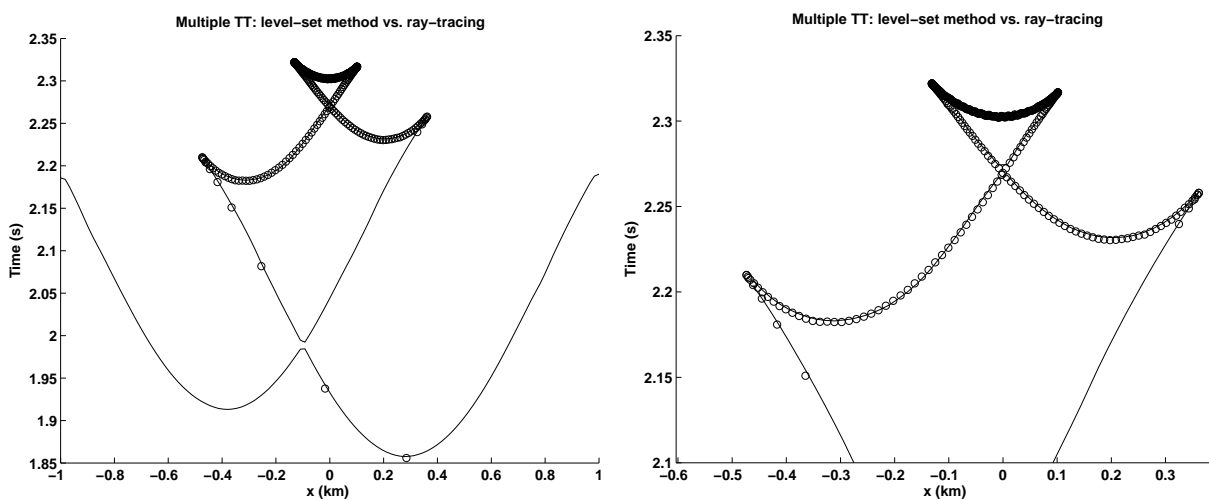


Figure 5: Eulerian traveltime ('-') computed on 120×120 mesh vs. Lagrangian traveltime ('o') by a ray tracing method at $z = 2.0$ in Sinusoidal model. The Eulerian approach captures more solutions than the ray tracing method.

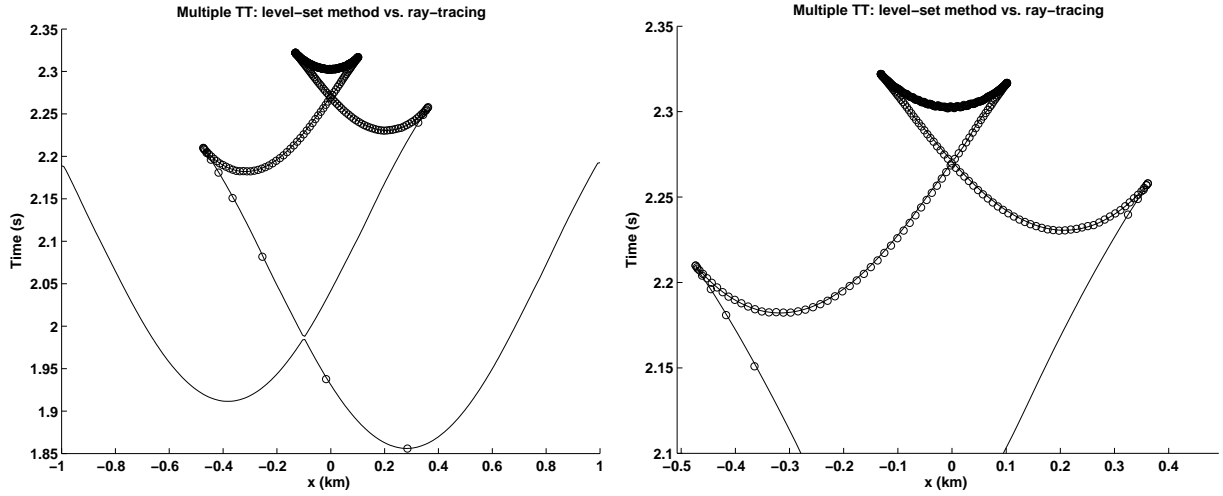


Figure 6: Eulerian traveltime ('-') computed on 240×240 mesh vs. Lagrangian traveltime ('o') by a ray tracing method at $z = 2.0$ in Sinusoidal model.

from the zero level set, receivers from 260 to 280 are single-valued functions of θ , and they correspond to first-arrival traveltimes. Apparently, the tip of the zero level set near receiver 260 should be more elongated, but somehow the level set failed to elongate that tip. This is partly due to the dissipation of the finite difference of the finite difference scheme used here and partly due to the resolution capability of the level set method which can resolve the zero level set only up to one grid-cell width. Computationally, if the segments of the zero level curve gets too close to each other, then they will merge and this is exactly happening to the tip that we are interested in.

Therefore, to resolve the fine tip we have to use a finer grid, 400×200 on $x-\theta$ space. Since the original velocity model is given on the discretized points, we use down-sampling (interpolation) to obtain a velocity model for the finer computational mesh. The computational results are shown on Figure 9 and 10. As we can see, in this run the level-set Eulerian method yields multivalued traveltimes which match with the ray tracing solution remarkably. From Figure 10, we can see that the zero level set does have an elongated tip from receiver 260 to 280, and the segments of the zero level set curve near the tip are indeed very close to each other. Without finer computational mesh, the level set method is unable to capture the tip and the related multivalued traveltimes.

6.5 An anisotropic model

Although a general anisotropic solid has 21 independent elastic parameters, the transversely isotropic, or TI, solid has only five. It nevertheless retains the essential features of the anisotropic case that we are interested in. Therefore, it is convenient to use TI solids as models to illustrate the advantages of our approach. We consider the simplest case for TI solids, those with vertical symmetry axes, known as VTI solids.

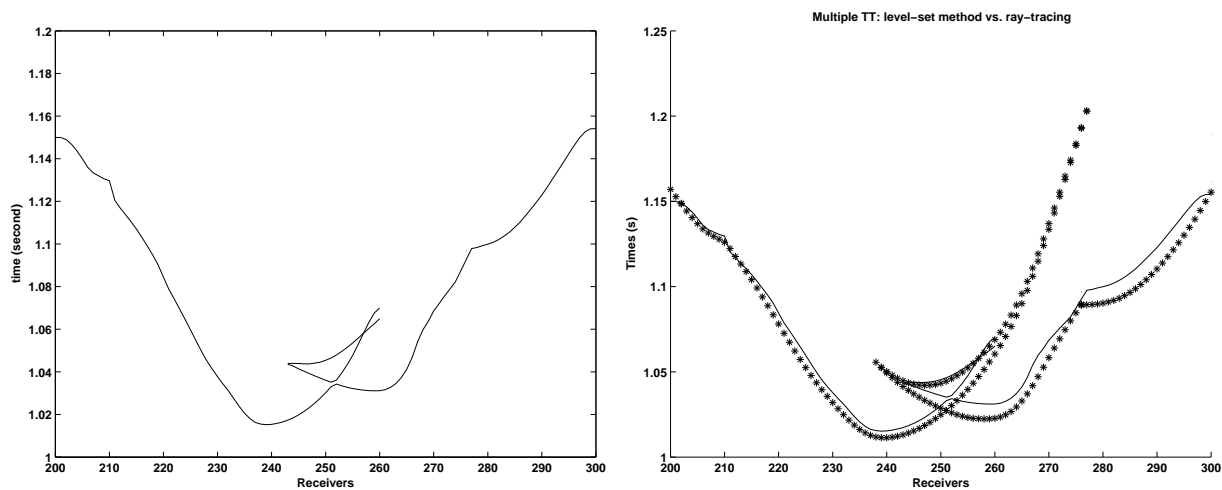


Figure 7: Left: traveltime at $z=0.0$ km by the level-set method for Marmousi model on 100×200 grid. Right: Eulerian traveltimes ('-') vs. ray-tracing traveltimes ('*')

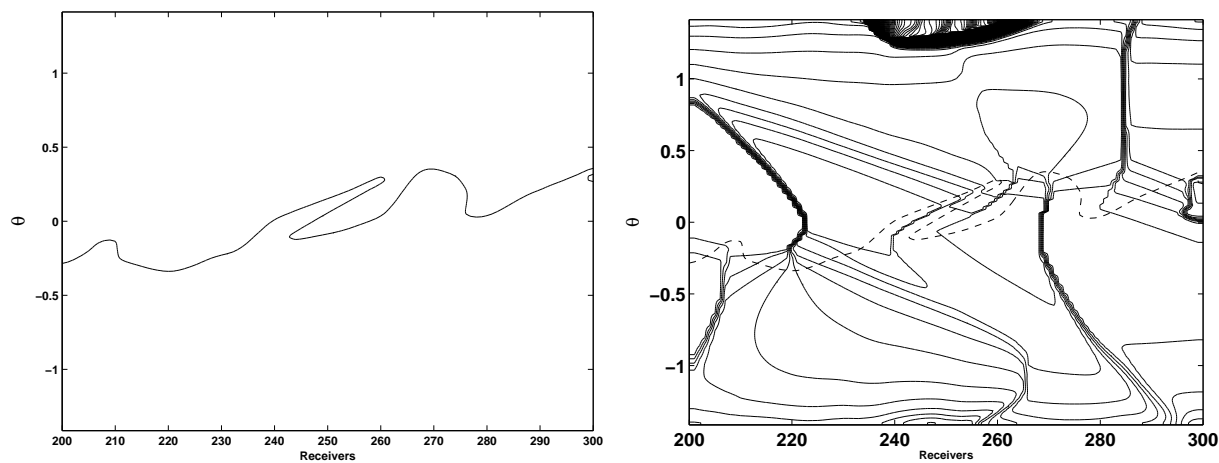


Figure 8: The zero level set for Marmousi model on 100×200 grid; the zero level set overlaying contours of T at $z=0.0$ km.

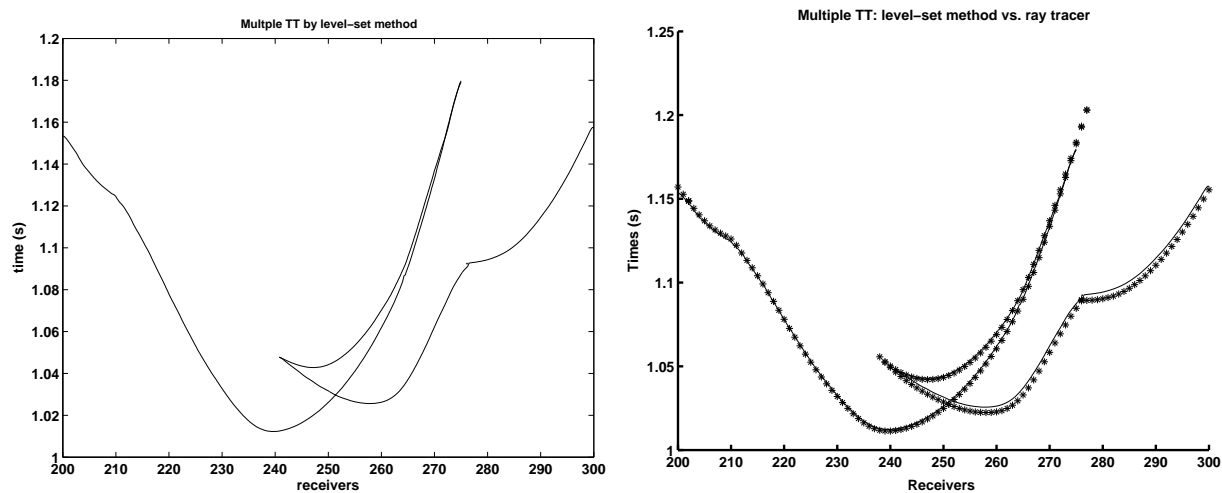


Figure 9: Left: traveltime at $z=0.0$ km by the level-set method for Marmousi model on 400×200 grid. Right: Eulerian traveltimes ('-') vs. ray-tracing traveltimes ('*')

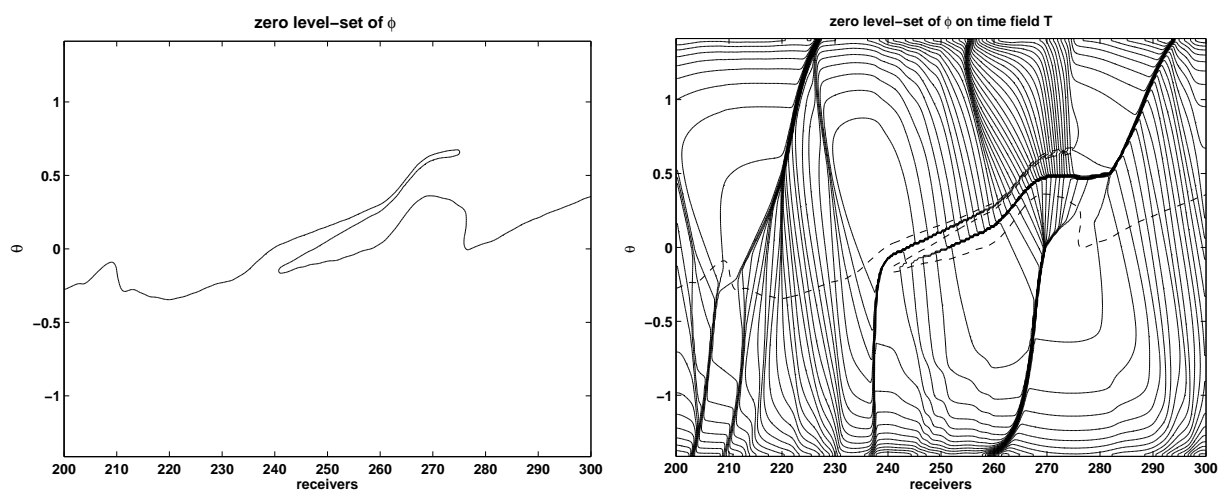


Figure 10: The zero level set for Marmousi model on 400×200 grid; the zero level set overlaying contours of T at $z=0.0$ km.

The elastic modulus matrix for transversely isotropic media with vertical symmetry axes has five independent components among a total of twelve nonzero components (see, e.g., [21]). A closed form solution exists in this case for the eigenvalue problem of so-called phase velocities. The quasi-P and quasi-SV slowness surfaces for VTI can be represented as a quartic polynomial equation and the quasi-SH slowness surface can be decoupled from this, leading to the equations [29]

$$c_1 p_1^4 + c_2 p_1^2 p_2^2 + c_3 p_2^4 + c_4 p_1^2 + c_5 p_2^2 + 1 = 0, \quad (53)$$

and

$$\frac{1}{2}(a_{11} - a_{12})p_1^2 + a_{44}p_2^2 = 1, \quad (54)$$

where

$$\begin{aligned} c_1 &\equiv a_{11}a_{44}, \\ c_2 &\equiv a_{11}a_{33} + a_{44}^2 - (a_{13} + a_{44})^2, \\ c_3 &\equiv a_{33}a_{44}, \\ c_4 &\equiv -(a_{11} + a_{44}), \\ c_5 &\equiv -(a_{33} + a_{44}). \end{aligned}$$

In the above equations, a_{ij} are independent elastic parameters of VTI media [21].

Thus, the phase velocities for the three different waves take the form

$$\begin{aligned} V_{qP}^2 &= \frac{1}{2} \left(-Y_1 + \sqrt{Y_1^2 - 4Y_2} \right), \\ V_{qSV}^2 &= \frac{1}{2} \left(-Y_1 - \sqrt{Y_1^2 - 4Y_2} \right), \\ V_{SH}^2 &= \frac{1}{2}(a_{11} - a_{12}) \sin^2 \theta + a_{44} \cos^2 \theta, \end{aligned}$$

where

$$\begin{aligned} Y_1 &= c_4 \sin^2 \theta + c_5 \cos^2 \theta, \\ Y_2 &= c_1 \sin^4 \theta + c_2 \cos^2 \theta \sin^2 \theta + c_3 \cos^4 \theta. \end{aligned}$$

As an example, we compute the three waves for Greenriver shale, which is a typical VTI medium [41]. The five elastic parameters are $a_{11} = 15.0638$, $a_{33} = 10.8373$, $a_{13} = 1.6381$, $a_{44} = 3.1258$, and $a_{12} = 6.5616$.

First we consider boundary conditions needed in this computation. For the level set equation we use the non-reflective boundary conditions just as that for the isotropic eikonal equation.

For the traveltimes equation, there need some extra efforts. Because the model is homogeneous and independent of x and z , the velocity component v in the level set equation is zero. Therefore, there is no need to specify any condition on the boundaries

$$\theta = \frac{\pi}{2} - \epsilon \text{ and } \theta = -\frac{\pi}{2} + \epsilon, \quad (55)$$

where ϵ is a small positive number. On the other two boundaries, analogous to the isotropic case, we can invert the characteristics locally and get

$$\frac{\partial T}{\partial x} = p_1 + \frac{p_3}{u}, \quad (56)$$

where u is another component in the velocity field of the level set equation. With the substitutions of p_1 and p_3 in terms of θ , we have the following differential equations needed to be solved numerically in order to determine the boundary conditions on the two boundaries $x = x_{\min}$ and $x = x_{\max}$,

$$\frac{\partial T}{\partial x} = \frac{1}{V} \left(\sin \theta + \frac{\cos \theta}{u} \right), \quad (57)$$

where V is the phase velocity of the wave mode that we are interested in.

Figure 11 shows traveltimes for the three different waves computed by the level set approach plotted in circles and comparisons with ray tracing solutions plotted in solid line at depth $z=0.5\text{km}$. These traveltimes are excited by a point source located at the origin. The upper-left sub-figure in Figure 11 shows the qP wave traveltime which is the fastest of the three waves. The lower-left sub-figure in Figure 11 shows the qSH wave traveltime. In particular, the qSV wave (the upper-right sub-figure in Figure 11) has cusps which imply the multivaluedness at some locations; those multivalued solutions are captured very well by the level set method. The lower-right sub-figure shows the three waves together.

7 Conclusion

We have applied the level set methodology to compute multivalued traveltimes in the paraxial formulation for both 2-D isotropic and anisotropic eikonal equations. The complexity of the proposed Eulerian method is $O(N^3)$ in the average case and $O(N^3 \text{Log} N)$ in the worst case. Numerical examples including the synthetic Marmousi model have demonstrated the accuracy and efficiency of the approach.

Although the formulation presented here is mainly for the point source condition, it will be valid for plane wave propagation too as long as the wave satisfies the sub-horizontal condition; however, we will not present examples here.

Future work includes computing the amplitude related to the multivalued traveltimes and implementing localized level set method [27] which will reduce the computational cost dramatically [30].

Acknowledgment

J. Qian thanks Professors S. Osher and W. W. Symes for many fruitful discussions. J. Qian and S. Leung were supported by ONR Grant #N00014-02-1-0720.

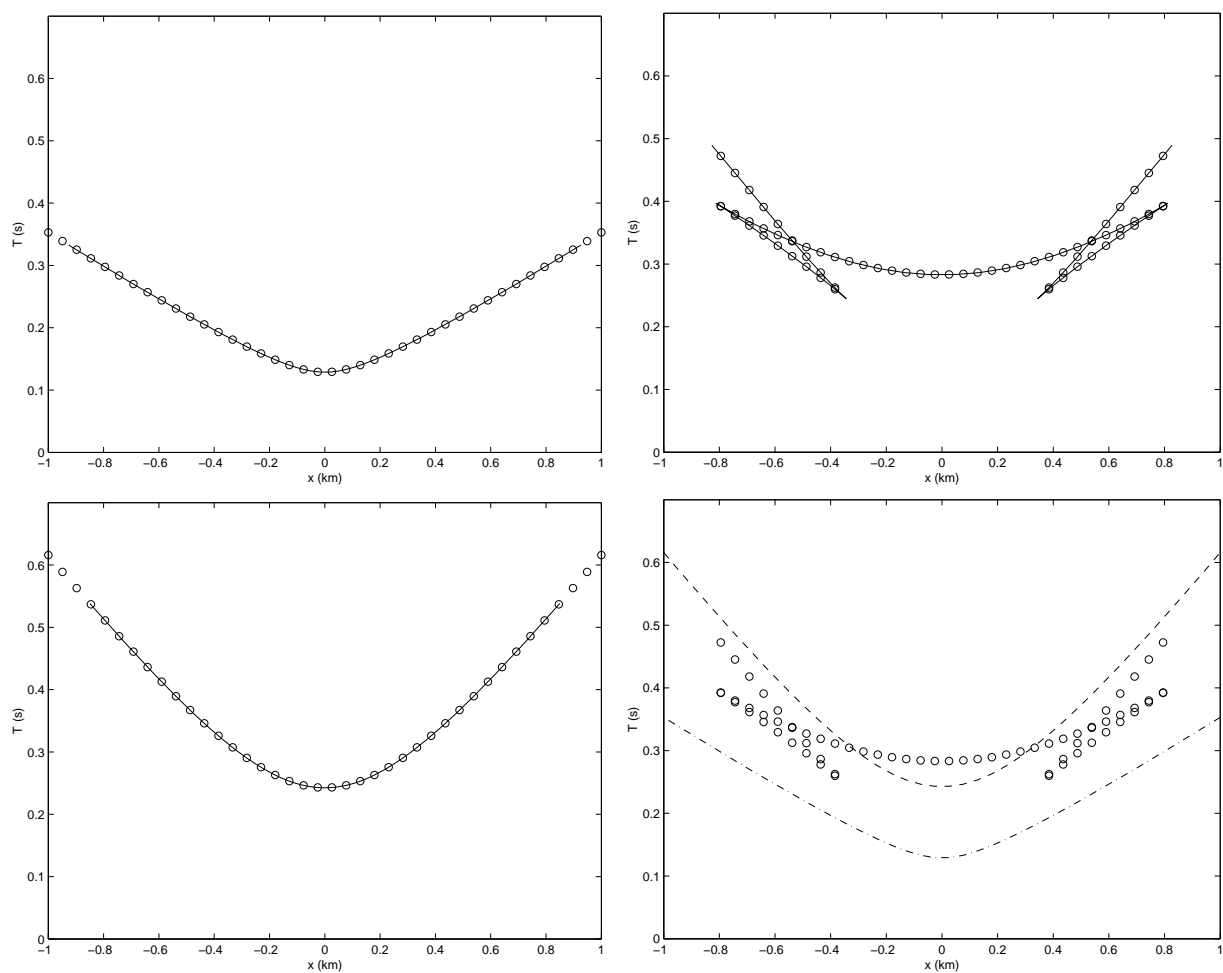


Figure 11: Anisotropic paraxial multivalued traveltimes by level set method. qP wave travel-time: the upper-left one; qSV traveltime: the upper-right one; qSH traveltime: the lower-left one; qP-qSV-qSH: the lower-right one.

Appendix

It comes to our attention that the formulation we used here is equivalent to a new formulation proposed in [18]. In this appendix, we will first derive a similar level set equation using the Jin-Osher formulation and then prove the equivalence of the two level set equations under the sub-horizontal condition.

We first rewrite the isotropic paraxial eikonal equation in the form of the following Hamilton-Jacobi equation

$$\frac{\partial t}{\partial z} - H(z, x, t_x) = 0 \quad (58)$$

with the Hamiltonian

$$H(z, x, t_x) = \sqrt{\frac{1}{c^2} - t_x^2}. \quad (59)$$

By differentiating the equation with respect to x and introducing $u = t_x$, we have

$$\frac{\partial u}{\partial z} - H_x(z, x, u) = 0. \quad (60)$$

To apply the level set method, we introduce a level set function $\psi = \psi(z, x, p)$ such that $\psi = 0$ gives the location of the ray with $p = u(z, x)$. Therefore, the corresponding level set equation can be obtained by differentiating $\psi(z, x, p(z, x))$ with respect to z and is given by

$$\psi_z + H_x \psi_p - H_p \psi_x = 0, \quad (61)$$

where H is given by equation (59). This provides another way for determining the multivalued solution of the eikonal equation. We can now solve this new level set equation, rather than the one we introduced in Section 4. By using similar procedures as in Algorithm 1, we determine all p_i such that $\psi(z^*, x^*, p_i) = 0$. With the relationship between p and θ

$$p = \frac{\sin \theta}{c(x, z)}, \quad (62)$$

we can then determine all the traveltimes from the traveltime equation (39).

However, it can be proven that two formulations are actually equivalent to each other. Defining $\psi(z, x, p) = \phi(z, x, \theta(p, x, z))$, we have the following change-of-variable relations

$$\begin{aligned} \frac{\partial \psi}{\partial z} &= \frac{\partial \phi}{\partial z} + \frac{\partial \phi}{\partial \theta} \frac{\partial \theta}{\partial z} \\ \frac{\partial \psi}{\partial p} &= \frac{\partial \phi}{\partial \theta} \frac{\partial \theta}{\partial p} \\ \frac{\partial \psi}{\partial x} &= \frac{\partial \phi}{\partial x} + \frac{\partial \phi}{\partial \theta} \frac{\partial \theta}{\partial x}, \end{aligned} \quad (63)$$

where

$$\frac{\partial\theta}{\partial z}, \frac{\partial\theta}{\partial p} \text{ and } \frac{\partial\theta}{\partial x}$$

are calculated by differentiating the Hamiltonian (59) with respect to z , p and x respectively. Now we can substitute these relations into the formulation (61) and get back our original level set equation (32).

References

- [1] J.-D. Benamou. Direct solution of multi-valued phase-space solutions for Hamilton-Jacobi equations. *Comm. Pure Appl. Math.*, 52:1443–1475, 1999.
- [2] J. D. Benamou. An introduction to Eulerian geometric optics. Preprint, 2002.
- [3] J.-D. Benamou and I. Sollic. A Eulerian method for capturing caustics. *J. Comput. Phys.*, 162:132–163, 2000.
- [4] Y. Brenier and L. Corrias. A kinetic formulations for multibranch entropy solutions of scalar conservation laws. *Ann. I.H.P. Nonlinear Anal.*, 15:169–190, 1998.
- [5] L.-T. Cheng, H. Liu, and S. J. Osher. High frequency wave propagation in Schrodinger equations using the level set method. Preprint (www.levelset.com), 2003.
- [6] J. F. Claerbout. *Imaging the Earth's interior*. Blackwell Scientific Pub., Palo Alto, CA, 1984.
- [7] R. Courant and D. Hilbert. *Methods of mathematical physics*, volume II. John Wiley-Sons, 1962.
- [8] M. G. Crandall, L. C. Evans, and P. L. Lions. Some properties of viscosity solutions of Hamilton-Jacobi equations. *Trans. Amer. Math. Soc.*, 282:487–502, 1984.
- [9] M. G. Crandall and P. L. Lions. Two approximations of solutions of Hamilton-Jacobi equations. *Math. Comp.*, 43:1–19, 1984.
- [10] B. Engquist, O. Runborg, and A-K Tornberg. High frequency wave propagation by the segment projection method. *J. Comp. Phys.*, 178:373–390, 2002.
- [11] S. Fomel and J. Sethian. Fast phase space computation of multiple traveltimes. *Proc. Nat. Aca. Sci.*, 99:7329–7334, 2002.
- [12] S. Geoltrain and J. Brac. Can we image complex structures with first-arrival traveltimes. *Geophysics*, 58:564–575, 1993.
- [13] L. Gosse. Using K-branch entropy solutions for multivalued geometric optics computations. *J. Comput. Phys.*, 180:155–182, 2002.

- [14] S. Gray and W. May. Kirchhoff migration using eikonal equation traveltimes. *Geophysics*, 59:810–817, 1994.
- [15] T. Y. Hou, Z. Li, S. J. Osher, and H.-K. Zhao. A hybrid method for moving interface problems with applications to the hele-shaw flows. *J. Comput. Phys.*, 134:236–252, 1997.
- [16] G. S. Jiang and D. Peng. Weighted ENO schemes for Hamilton-Jacobi equations. *SIAM J. Sci. Comput.*, 21:2126–2143, 2000.
- [17] S. Jin and X. Li. Multi-phase computations of the semi-classical limit of the Schrodinger equation and related problems. *Physica D* (in press), 2003.
- [18] S. Jin and S. Osher. A level set method for the computation of multivalued solutions to quasi-linear hyperbolic PDEs and Hamilton-Jacobi equations. Preprint (www.levelset.com), 2003.
- [19] P. L. Lions. *Generalized solutions of Hamilton-Jacobi equations*. Pitman Advanced Publishing Program, 1982.
- [20] Z. Liu and N. Bleistein. Migration velocity analysis: theory and an iterative algorithm. *Geophysics*, 60:142–153, 1995.
- [21] M. J. P. Musgrave. *Crystal acoustics*. Holden-Day, 1970.
- [22] S. Operto, S. Xu, and G. Lambare. Can we image quantitatively complex models with rays. *Geophysics*, 65:1223–1238, 2000.
- [23] S. Osher, L.-T. Cheng, M. Kang, H. Shim, and Y-H Tsai. Geometrical optics in a phase space based level set and Eulerian framework. *J. Comput. Phys.*, 179:622–648, 2002.
- [24] S. Osher and R. P. Fedkiw. *The Level Set Method and Dynamic Implicit Surfaces*. Springer-Verlag, New York, 2002.
- [25] S. J. Osher and J. A. Sethian. Fronts propagating with curvature dependent speed: algorithms based on Hamilton-Jacobi formulations. *J. Comput. Phys.*, 79:12–49, 1988.
- [26] S. J. Osher and C. W. Shu. High-order Essentially NonOscillatory schemes for Hamilton-Jacobi equations. *SIAM J. Num. Anal.*, 28:907–922, 1991.
- [27] D. Peng, B. Merriman, S. Osher, H. K. Zhao, and M. Kang. A pde-based fast local level set method. *J. Comput. Phys.*, 155:410–438, 1999.
- [28] F. Poupaud and C. Ringhofer. Semi-classical limits in a crystal with external potentials and effective mass theorems. *Commun. Partial Diff. Eq.*, 21:1897–1918, 1996.
- [29] J. Qian, L.-T. Cheng, and S.J. Osher. A level set based Eulerian approach for anisotropic wave propagations. *Wave Motion*, 37:365–379, 2003.

- [30] J. Qian and S. Leung. A local level method for paraxial multivalued geometric optics. In preparation, 2003.
- [31] J. Qian and W. W. Symes. Adaptive finite difference method for traveltime and amplitude. *Geophysics*, 67:167–176, 2002.
- [32] J. Qian and W. W. Symes. Finite-difference quasi-P traveltimes for anisotropic media. *Geophysics*, 67:147–155, 2002.
- [33] E. Rouy and A. Tourin. A viscosity solutions approach to shape-from-shading. *SIAM J. Num. Anal.*, 29:867–884, 1992.
- [34] S. J. Ruuth, B. Merriman, and S. J. Osher. A fixed grid method for capturing the motion of self-intersecting interfaces and related PDEs. *J. Comput. Phys.*, 151:836–861, 1999.
- [35] C. Sparber, P. Markowich, and N. Mauser. Multivalued geometrical optics: Wigner functions vs. WKB methods. *Asymptotic Anal.*, 33:153–197, 2003.
- [36] J. Steinhoff, M. Fan, and L. Wang. A new Eulerian method for the computation of propagating short acoustic and electromagnetic pulses. *J. Comput. Phys.*, 157:683–706, 2000.
- [37] M. Sussman, P. Smereka, and S. J. Osher. A level set approach for computing solutions to incompressible two-phase flows. *J. Comput. Phys.*, 114:146–159, 1994.
- [38] W. W. Symes. Mathematics of reflection seismology. In *Annual Report, The Rice Inversion Project*, (<http://www.trip.caam.rice.edu/>). Rice University, 1995.
- [39] W. W. Symes. A slowness matching finite difference method for traveltimes beyond transmission caustics. In *68th Ann. Internat. Mtg., Soc. Expl. Geophys., Expanded Abstracts*, pages 1945–1948. Soc. Expl. Geophys., 1998.
- [40] W. W. Symes and J. Qian. A slowness matching Eulerian method for multivalued solutions of eikonal equations. *J. Sci. Comp.* (in press), 2003.
- [41] L. Thomsen. Weak elastic anisotropy. *Geophysics*, 51:1954–1966, 1986.
- [42] V. Vinje, E. Iversen, and H. Gjystdal. Traveltime and amplitude estimation using wavefront construction. *Geophysics*, 58:1157–1166, 1993.
- [43] B. S. White. The stochastic caustic. *SIAM J. Appl. Math.*, 44:127–149, 1984.